years (range, 22–78), and median Karnofsky Performance Scale (KPS) was 70 (30–80) (Table 1). Five patients underwent RT plus concomitant TMZ at the initial therapy, and others received TMZ monotherapy on disease progression. BV treatment was primarily (67 %) given as the second line therapy (range 2–5). The cycles of BV therapy ranged from 1 to 21 (median 7). There were no serious adverse events in any of the patients.

Response to BV

After the first BV cycle, early post-treatment MR imaging (taken between days 3 and 21, median 13) demonstrated rapid shrinkage of both enhancing and T2-elongated (hyperintense on T2-weighted and FLAIR images) areas in most tumors (Fig. 1). By a patient-based analysis, single BV treatment resulted in a decrease in evaluable enhancing tumor volume in eight of nine cases (88.9 %) (Table 1). Four patients (44.4 %) had a partial response (PR), four had a stable disease (SD), and one had a progressive disease (PD) by the Macdonald criteria; the overall response rate was 44.4 %. In cases 1, 3, and 8, both hemiparesis and disturbance of consciousness recovered soon after the first BV administration with a marked reduction of extent of hyperintensity on T2-weighted or FLAIR images along with the enhancing tumor shrinkage. KPS improved immediately in four cases (44.4 %).

Association of tumor mADC values with the response to BV

Of 15 individual evaluable enhancing lesions in the nine patients, 11 tumors shrank (Fig. 1), while four did not respond upon initial BV treatment (Fig. 2). We then evaluated parameters obtained in the MR images to determine if there were any predictors for tumor response to BV. The pretreatment MR images were obtained on days −1 to −25 (median −10). The average pretreatment mADC value for all lesions was 1249 (10^{-6} mm^2/s) (range 964–1672). Tumor mADC values were above 1100 in all of the responding tumors, in contrast to those in all non-responding lesions that scored below 1100 (Fisher's exact test, $p = 0.001$) (Fig. 3), suggesting that a pretreatment mADC value higher than 1100 may be predictive for a rapid shrinkage of enhancing tumors. Interestingly, the tumor mADC values decreased significantly after the first BV treatment in all lesions except for one that did not respond (paired t test, $p < 0.001$) (Fig. 4). The average mADC value after the first cycle of BV was 1051 (range 828–1320).

To determine whether the mADC value after the first BV treatment (post-BV mADC) could also predict a further response of the lesion to additional cycles of BV, the ratio

Table 1 Summary of cases treated with bevacizumab monotherapy on temozolomide failure

No	Age (years)	Gender	KPS (pre-BV)	Pathological Dx	RT (Gy)	TMZ cycles	TMZ OR	*MGMT* status	BV line[a]	BV cycles	Months from last RT	mADC (pre-BV) (10^{-6} mm^2/s)	Total TV (ml) (pre-BV)	BV OR	Relative TV[b]	KPS (post 1st BV)	Relapse	PFS (months)	Out-come	OS (months)
1	74	Female	40	AA	60	46	CR	nd	3	7	77	1394	61.7	SD	0.63	50	+	2.2	D	5.7
2	51	Male	70	AA	60 + SRT	14	SD	nd	2	21	15.2	1354	45.0	PR	0.03	70	+	7.7	D	16.0
3	60	Female	70	GBM	60 + SRT	11	SD	M	2	4	5.6	964–1490[c]	25.7	SD	0.88	90	+	1.5	D	3.3
4	32	Female	70	GBM-s	50	10	SD	M	3	8	35.8	1190	23.7	SD	0.73	70	+	2.3	D	5.5
5	22	Male	80	GBM-s	60	1	PD	U	2	12	2.1	1273	16.8	PR	0.13	80	+	5.5	D	10.3
6	73	Female	60	GBM	60	5	SD	U	2	1	6.7	1009–1281[c]	7.9	PD	1.78	50	+	0.4	D	3.9
7	58	Female	80	GBM	60	8	SD	U	2	8	7.6	1323	8.4	PR	0.67	80	+	3.9	D	11.1
8	51	Female	30	GBM	60 + SRT	40	CR	M	5[a]	5	4.3	1281	152.8	SD	0.54	50	+	1.4	D	2.9
9	78	Male	30	GBM	40	1	PD	U	2	3	1.9	1257–1672[c]	72.9	PR	0.24	40	+	2.1	D	8.3

KPS Karnofsky Performance Scale, *Dx* diagnosis, *RT* radiotherapy, *TMZ* temozolomide, *OR* objective response, *MGMT* O^6-methylguanine-DNA methyltransferase, *BV* bevacizumab, *mADC* mean apparent diffusion coefficient, *pre-BV* before the first BV treatment, *TV* tumor volume, *PFS* progression-free survival, *OS* overall survival, *AA* anaplastic astrocytoma, *GBM* glioblastoma, *GBM-s*, secondary GBM, *SRT* stereotactic radiotherapy, *CR* complete response, *PR* partial response, *SD* stable disease, *PD* progressive disease, *nd* not determined, *M* methylated promoter, *U* unmethylated promoter, *D*, dead

[a] Previous chemotherapy included bevacizumab

[b] The ratio of tumor volume at the first MR imaging post-bevacizumab treatment compared with that of the baseline

[c] The lowest and highest values of multiple lesions

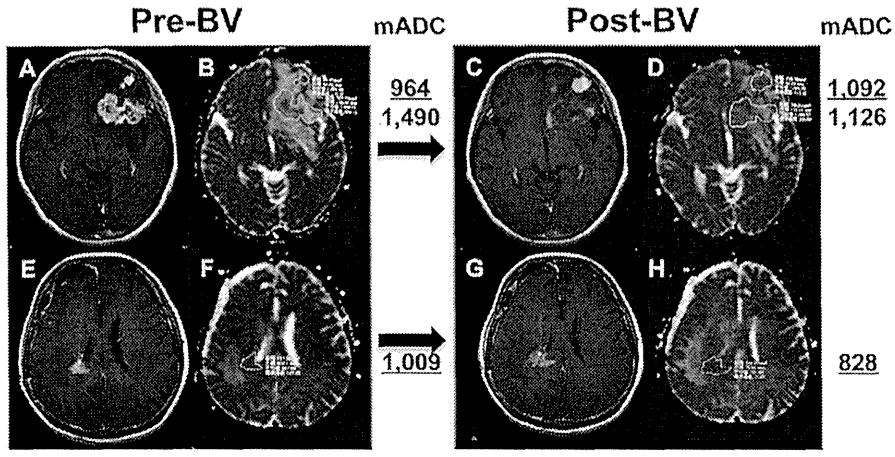

Fig. 2 Post-contrast T1-weighted images aligned side-by-side with the corresponding ADC maps in patients with tumors which did not respond to BV (**a, b, c, d**: case 3; **e, f, g, h**: case 6). Note that the non-responding lesions have mADC values below 1100 (10^{-6} mm^2/s). In case 3, the anterior frontal lesion with an initial mADC of 964 continues to grow, whereas the posterior frontal lesion that has undergone stereotactic radiotherapy before further progression shows an initial mADC of 1490 and its enhancement reduces after BV treatment

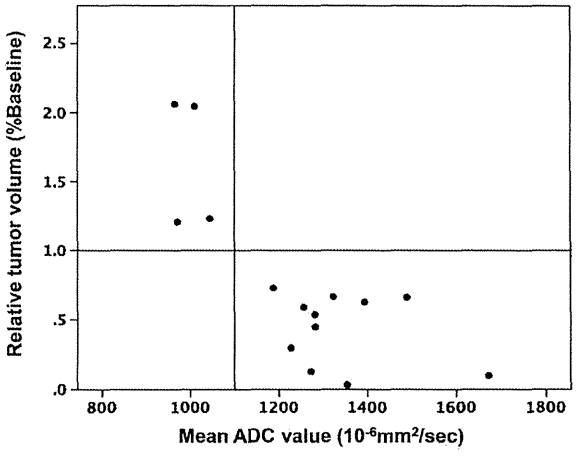

Fig. 3 Clear correlation between mean ADC values and changes in tumor size after a single BV treatment in recurrent high-grade glioma lesions. All lesions with mADC above 1100 (10^{-6} mm^2/s) shrink, while those with lower mADC continue growth (Fisher's exact test, $p = 0.001$)

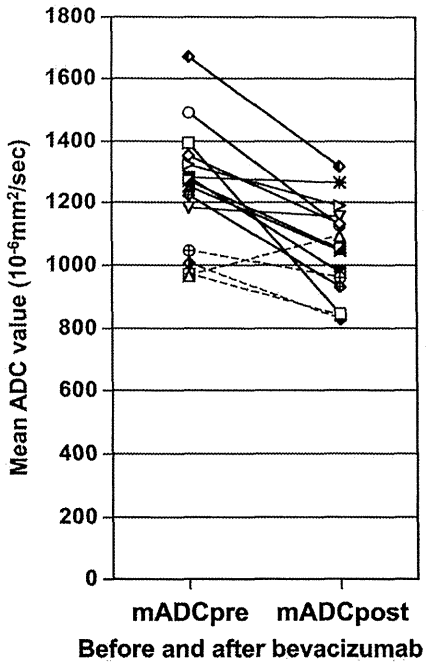

Fig. 4 Changes in mADC value between pre- and post-treatment with BV. Corresponding mADC value points of each lesion are connected with *lines*; the responding lesions are in *solid lines* and the non-responding are in *dashed lines*. mADC values of all lesions decrease after BV except for one non-responding

of tumor volumes at the first MR imaging to those at the second MR imaging taken after 2 more BV cycles (median interval, 39 days; range, 35–56 days) was measured (Table 2). Post-BV mADC significantly correlated with response to additional BV (Mann–Whitney U test, $p = 0.045$) and all five high post-BV mADC (>1100) lesions shrank after the additional BV treatments. Although three of eight (37.5 %) low post-BV mADC (<1100) lesions also decreased in size, the majority (5/8, 62.5 %) did not respond further, which approached statistical significance (Fisher's exact test; $p = 0.075$). These observations suggest that even the mADC immediately after the first BV treatment may be of predictive value for further response to BV.

Table 2 mADC values before and after the first bevacizumab treatment and the change in tumor volume

Case	Lesion	mADC (10^{-6} mm^2/s)		TV (%baseline) (1st F/U MRI)	TV (%baseline) (2nd F/U MRI)	TV (%1st MRI) (2nd F/U MRI)
		Before	After			
1	P/T	1394.2	842.5	62.7	21.8	34.9
2	T	1353.6	1135.8	3.3	0.0	0.0
3	F	1490.1	1125.6	66.1	63.6	96.3
	F-AL	964.3	1092.0	206.4	445.5	215.9
	F-AM	971.1	841.1	120.9	135.5	112.1
	F-MF	1227.6	930.0	29.8	30.4	103.1
	F-PM	1044.5	961.8	123.2	225.6	183.1
4	F-BG	1187.5	1155.4	72.8	15.2	20.9
5	T	1272.6	1053.0	12.9	0.0	0.0
6	T	1008.9	827.6	204.6	na	na
	F	1281.1	1267.7	44.8	na	na
7	CC	1323.4	1192.9	66.5	18.3	27.9
8	PT	1280.9	977.4	53.8	106.7	198.4
9	F	1672.4	1320.5	10.0	7.3	73.7
	F	1256.7	1046.5	58.9	50.1	85.1

TV, tumor volume, *F/U* follow-up, *P* parietal, *T* temporal, *F* frontal, *AL* antero-lateral, *AM* antero-medial, *MF* mid-frontal, *PM* premotor, *BG* basal ganglia, *CC* corpus callosum

Survival

After a median follow-up of 5.7 months (range, 2.9–16.0), all patients had progressed and died despite a high rate of early response. PFS from the initiation of BV therapy was 2.2 months [95 % confident interval (CI) 1.8–2.6 months]. PFS for two patients (cases 3 and 6) having a lesion with mADC value <1100 (low mADC) was short (0.4 months), whereas PFS for others having all lesions with mADC >1100 (high mADC) was significantly longer (2.3 months, 95 % CI 2.0–2.6) (log-rank test, $p = 0.018$). Median OS after the start of BV treatment was 5.7 months (95 % CI 5.1–6.2). Patients having all lesions with a high mADC (>1100) survived significantly longer (median 8.3 months, 95 % CI 1.4–15.2) than those with a low mADC tumor(s) (median 3.3 months, $p = 0.046$), despite the small sample number (9 cases). The tumor volume of enhancing lesions prior to initiation of BV was not associated with either PFS or OS (Table 1, data not shown).

VEGF expression in the original tumor specimens

Immunohistochemistry staining of VEGF-A was performed in the primary tumors and all but one were found to express VEGF to a variable extent (data not shown). Expression at the beginning of BV treatment was not determined due to lack of re-resection prior to BV therapy. The tumor with negative VEGF staining (case 6) did not respond to BV.

Relationship of mADC with *MGMT* promoter methylation status

While *MGMT* status is prognostic/predictive for survival in GBM patients [17, 18], tumoral mADC values were not associated with *MGMT* methylation status (Fisher's exact test; $p = 0.445$) in the seven GBM cases (Table 1). Taken together, while we observed that response of recurrent lesions after a single dose of BV was significantly correlated with a mean ADC value of the tumors above 1100 (10^{-6}mm^2/s), it was not with VEGF expression or *MGMT* status.

Discussion

Although BV has shown efficacy against TMZ-refractory GBMs, some tumors may also be resistant to BV, progressing to fatality [19], and thus determining their sensitivity to BV prior to initiation of the treatment could have significant clinical value. Here, we demonstrated that the pretreatment mADC value of enhancing tumors was predictive for initial response to BV monotherapy in recurrent HGGs. All lesions with the mADC above 1100 (10^{-6} mm^2/s) responded, in clear contrast to those with the mADC below 1100, which did not respond ($p = 0.001$) (Fig. 3). The mADC values decreased after the first BV treatment in all lesions, except for one that did not respond. The second mADC value obtained after the first BV treatment was also a good indicator for further response to additional BV when it remained above 1100 ($p = 0.045$). Furthermore, the high mADC value also significantly correlated with elongation of both PFS and OS after BV treatment in patients with TMZ-refractory recurrent HGGs.

Anti-VEGF therapy is expected to normalize vascular structure, capillary permeability and interstitial pressure more effectively in areas with strong edema and necrotic changes than in those with "packed" tumor cells. The ADC value represents movement of protons of water molecules and may be increased in areas where tissue edema and necrotic components have been induced by tissue damage from tumor burden and cytotoxic therapies [9–11]. This may account for our findings that glioma lesions with a high pretreatment ADC value shrank upon BV challenge whereas those with a low ADC value did not. Such non-responding lesions also tended to be strongly enhanced (e.g., a subcortical lesion in the left frontal lobe in Fig. 2a), consistent with the observation that GBMs that relapsed after BV treatment exhibited low ADC values and hyperintensity on diffusion-weighted images [20].

Pope et al. reported that PFS correlated with crude average ADC values within areas showing contrast enhancement in 41 recurrent GBM cases who underwent BV treatment. Of note, when the average ADC value of the lower peak of biphasic peaks in ADC histograms ($mADC_L$) was lower than 1201, PFS was significantly extended [21]. Our use of whole ADC values within an enhancing tumor to calculate a mean value on a PACS terminal in clinics without specific software successfully segregated responding from non-responding lesions. This simple method might incorporate regions of extremely high ADC values containing necrotic tissues, resulting in a shift of the mean value toward a higher value, compared with the histogram-based analysis. However, regions exhibiting apparent necrosis or cyst could be readily excluded when defining a tumor on each ADC map, in order to avoid such data contamination. We also eliminated T2-elongated areas surrounding contrast-enhancing lesions because they may contain both edematous white matter and non-enhancing tumor to a variable extent. As a result, our data show clear segregation of lesions for response by ADC value at 1100 (10^{-6} mm^2/s), smaller than the cut-off value of 1201 in the Pope study [21]. It would be beneficial in daily practice to use this simple measurement, as it does not require specific histogram analysis, though it needs further accumulation of cases for validation.

Conflicting findings that BV induces rapid shrinkage of the enhancing lesions while they subsequently regrow in a relatively short term might represent, at least partly, the recently recognized "pseudo-response," a decrease in enhancing tumor on MR imaging without a decrease in tumor activity [22]. This has been reported in a clinical trial where radiation necrosis was successfully treated with BV [23]. To date, there are no validated imaging methods to determine whether the observed shrinkage of areas of contrast enhancement were due to real tumor reduction or pseudo-response, as well as progression without an emergence or increase of enhancing lesion [24]. Indeed, the potential value of changes in T2 relaxation time is recently suggested by an observation that an elevated residual, post-treatment, median T2 may be predictive of both PFS and OS [25]. Efforts to clarify these issues include application of the newly-developed response criteria, Response Assessment in Neuro-Oncology (RANO), utilizing elongation of T2 relaxation time as a surrogate for non-enhancing tumor [26], and MR imaging techniques such as MR perfusion studies that are under investigation in large trials for validity. In our study, there were two patients (cases 3 and 8) who underwent stereotactic RT on recurrence prior to BV initiation, and one patient (case 5) who received BV within 3 months after completion of induction-concomitant RT plus TMZ. Two of these three patients had a PR by single BV treatment with further progression in 2 and 5.5 months, indicating no clear relationship between response and potential radiation injury.

A recent study reported that the lower ADC_L value rather correlated with longer PFS for patients with newly-diagnosed GBM [27], in contrast to recurrent GBM. It also showed an association between ADC values and *MGMT* methylation status [27], which was not observed in our series. Whether this association might be influenced by the difference of tumor microstructure in the setting of newly-diagnosed or treatment-modified recurrent tumors needs to be clarified.

Limitations of our study include the small number of patients and lesions analyzed, heterogeneous prior treatment regimens applied in some patients, and specimens from primary newly-diagnosed tumors used for determination of VEGF and *MGMT* status. This might hamper drawing definite conclusions about the relationship of the mADC value with survival gain or VEGF/*MGMT* status, as well as analyzing whether pathological findings of treated tumors may also correlate with either mADC values or responsiveness to BV, or both. However, even with the small sample size, a clear segregation of responders from non-responders and survival prediction were seen using our simplified mADC measurement and this warrants further investigation in a larger series.

Conclusions

Bevacizumab monotherapy is an active regimen for patients with TMZ-refractory recurrent gliomas leading to rapid lesion shrinkage, and the tumor mADC value can be a useful marker for prediction of BV response and survival, and thus for patient selection. It would be also intriguing to investigate methods of delineating tumors in which BV would provide long-term response in the future.

Acknowledgments This work was supported partially by grants of the Ministry of Health, Labour, and Welfare of Japan (H20-ganrins-you-ippan-019 and 20shi-4) (to MN). We thank Kuninori Kobayashi, RT (Radiology Section, Kyorin University Hospital) for obtaining MR imaging data.

Conflict of interest The authors declare that they have no conflict of interest.

References

1. Stupp R, Mason WP, van den Bent MJ et al (2005) Radiotherapy plus concomitant and adjuvant temozolomide for glioblastoma. N Engl J Med 352:987–996
2. Norden AD, Drappatz J, Wen PY (2009) Antiangiogenic therapies for high-grade glioma. Nat Rev Neurol 5:610–620

3. Fischer I, Gagner JP, Law M et al (2005) Angiogenesis in gliomas: biology and molecular pathophysiology. Brain Pathol 15:297–310
4. Yuan F, Chen Y, Dellian M et al (1996) Time-dependent vascular regression and permeability changes in established human tumor xenografts induced by an anti-vascular endothelial growth factor/vascular permeability factor antibody. Proc Natl Acad Sci USA 93:14765–14770
5. Chamberlain MC (2010) Emerging clinical principles on the use of bevacizumab for the treatment of malignant gliomas. Cancer 116:3988–3999
6. Vredenburgh JJ, Desjardins A, Herndon JE 2nd et al (2007) Bevacizumab plus irinotecan in recurrent glioblastoma multiforme. J Clin Oncol 25:4722–4729
7. Friedman HS, Prados MD, Wen PY et al (2009) Bevacizumab alone and in combination with irinotecan in recurrent glioblastoma. J Clin Oncol 27:4733–4740
8. Kreisl TN, Kim L, Moore K et al (2009) Phase II trial of single-agent bevacizumab followed by bevacizumab plus irinotecan at tumor progression in recurrent glioblastoma. J Clin Oncol 27:740–745
9. Sugahara T, Korogi Y, Kochi M et al (1999) Usefulness of diffusion-weighted MRI with echo-planar technique in the evaluation of cellularity in gliomas. J Magn Reson Imaging 9:53–60
10. Mardor Y, Roth Y, Ochershvilli A et al (2004) Pretreatment prediction of brain tumors' response to radiation therapy using high b-value diffusion-weighted MRI. Neoplasia 6:136–142
11. Chenevert TL, Sundgren PC, Ross BD (2006) Diffusion imaging: insight to cell status and cytoarchitecture. Neuroimaging Clin N Am 16:619–632 viii-ix
12. Oh J, Henry RG, Pirzkall A et al (2004) Survival analysis in patients with glioblastoma multiforme: predictive value of choline-to-*N*-acetylaspartate index, apparent diffusion coefficient, and relative cerebral blood volume. J Magn Reson Imaging 19:546–554
13. Murakami R, Sugahara T, Nakamura H et al (2007) Malignant supratentorial astrocytoma treated with postoperative radiation therapy: prognostic value of pretreatment quantitative diffusion-weighted MR imaging. Radiology 243:493–499
14. Higano S, Yun X, Kumabe T et al (2006) Malignant astrocytic tumors: clinical importance of apparent diffusion coefficient in prediction of grade and prognosis. Radiology 241:839–846
15. Macdonald DR, Cascino TL, Schold SC Jr et al (1990) Response criteria for phase II studies of supratentorial malignant glioma. J Clin Oncol 8:1277–1280
16. Nagane M, Nozue K, Shimizu S et al (2009) Prolonged and severe thrombocytopenia with pancytopenia induced by radiation-combined temozolomide therapy in a patient with newly diagnosed glioblastoma—analysis of O^6-methylguanine-DNA methyltransferase status. J Neurooncol 92:227–232
17. Hegi ME, Diserens AC, Gorlia T et al (2005) MGMT gene silencing and benefit from temozolomide in glioblastoma. N Engl J Med 352:997–1003
18. Nagane M, Kobayashi K, Ohnishi A et al (2007) Prognostic significance of O6-methylguanine-DNA methyltransferase protein expression in patients with recurrent glioblastoma treated with temozolomide. Jpn J Clin Oncol 37:897–906
19. Wong ET, Brem S (2008) Antiangiogenesis treatment for glioblastoma multiforme: challenges and opportunities. J Natl Compr Canc Netw 6:515–522
20. Gerstner ER, Frosch MP, Batchelor TT (2010) Diffusion magnetic resonance imaging detects pathologically confirmed, nonenhancing tumor progression in a patient with recurrent glioblastoma receiving bevacizumab. J Clin Oncol 28:e91–e93
21. Pope WB, Kim HJ, Huo J et al (2009) Recurrent glioblastoma multiforme: ADC histogram analysis predicts response to bevacizumab treatment. Radiology 252:182–189
22. Brandsma D, van den Bent MJ (2009) Pseudoprogression and pseudoresponse in the treatment of gliomas. Curr Opin Neurol 22:633–638
23. Levin VA, Bidaut L, Hou P et al (2011) Randomized double-blind placebo-controlled trial of bevacizumab therapy for radiation necrosis of the central nervous system. Int J Radiat Oncol Biol Phys 79:1487–1495
24. Pope WB, Young JR, Ellingson BM (2011) Advances in MRI assessment of gliomas and response to anti-VEGF therapy. Curr Neurol Neurosci Rep 11:336–344
25. Ellingson BM, Cloughesy TF, Lai A et al (2012) Quantification of edema reduction using differential quantitative T2 (DQT2) relaxometry mapping in recurrent glioblastoma treated with bevacizumab. J Neurooncol 106:111–119
26. Wen PY, Macdonald DR, Reardon DA et al (2010) Updated response assessment criteria for high-grade gliomas: response assessment in neuro-oncology working group. J Clin Oncol 28:1963–1972
27. Pope WB, Lai A, Mehta R et al (2011) Apparent diffusion coefficient histogram analysis stratifies progression-free survival in newly diagnosed bevacizumab-treated glioblastoma. AJNR Am J Neuroradiol 32:882–889

Miwa et al. Radiation Oncology 2014, 9:181
http://www.ro-journal.com/content/9/1/181

RADIATION ONCOLOGY

RESEARCH Open Access

Re-irradiation of recurrent glioblastoma multiforme using ^{11}C-methionine PET/CT/MRI image fusion for hypofractionated stereotactic radiotherapy by intensity modulated radiation therapy

Kazuhiro Miwa[1,5*], Masayuki Matsuo[2], Shin-ichi Ogawa[2], Jun Shinoda[1], Kazutoshi Yokoyama[3], Jitsuhiro Yamada[3], Hirohito Yano[4] and Toru Iwama[4]

Abstract

Background: This research paper presents a valid treatment strategy for recurrent glioblastoma multiforme (GBM) using hypofractionated stereotactic radiotherapy by intensity modulated radiation therapy (HS-IMRT) planned with ^{11}C-methionine positron emission tomography (MET-PET)/computed tomography (CT)/magnetic resonance imaging (MRI) fusion.

Methods: Twenty-one patients with recurrent GBM received HS-IMRT planned by MET-PET/CT/MRI. The region of increased amino acid tracer uptake on MET-PET was defined as the gross tumor volume (GTV). The planning target volume encompassed the GTV by a 3-mm margin. Treatment was performed with a total dose of 25- to 35-Gy, given as 5- to 7-Gy daily for 5 days.

Results: With a median follow-up of 12 months, median overall survival time (OS) was 11 months from the start of HS-IMRT, with a 6-month and 1-year survival rate of 71.4% and 38.1%, respectively. Karnofsky performance status was a significant prognostic factor of OS as tested by univariate and multivariate analysis. Re-operation rate was 4.8% for radiation necrosis. No other acute or late toxicity Grade 3 or higher was observed.

Conclusions: This is the first prospective study of biologic imaging optimized HS-IMRT in recurrent GBM. HS-IMRT with PET data seems to be well tolerated and resulted in a median survival time of 11 months after HS-IMRT.

Keywords: Recurrent glioblastoma multiforme, Hypofractionated stereotactic radiotherapy, Intensity modulated radiation therapy, ^{11}C-methionine PET

Background

In recurrent gliomas retreated with radiation therapy, precise dose delivery is extremely important in order to reduce the risk of normal brain toxicity. Recently, novel treatment modalities with increased radiation dose-target conformality, such as intensity modulated radiation therapy (IMRT), have been introduced [1-4]. While IMRT has superior target isodose coverage compared to other external radiation techniques in scenarios involving geometrically complex target volumes adjacent to radiosensitive tissues, planning and delivery in IMRT are resource intensive and require specific and costly software and hardware.

Gross tumor volume (GTV) delineation in gliomas has been traditionally based on computed tomography (CT) and magnetic resonance imaging (MRI). However, ^{11}C-methionine positron emission tomography (MET-PET) for high-grade gliomas was recently demonstrated to have an improved specificity and sensitivity and is the

* Correspondence: kz-surg.21@gero-hp.jp
[1]Chubu Medical Center for Prolonged Traumatic Brain Dysfunction, Kizawa Memorial Hospital, Minokamo, Gifu, Japan
[5]Department of Neurosurgery, Chubu Medical Center for Prolonged Traumatic Brain Dysfunction, 630 Shimokobi, Kobi-cho, Minokamo, Gifu 505-0034, Japan
Full list of author information is available at the end of the article

rationale for the integration of biologic imaging in the treatment planning [5-8]. In previous studies using MET-PET/MRI image fusion, we demonstrated that biologic imaging helps to detect tumor infiltration in regions with a non-specific MRI appearance in a significant number of patients [9-11]. Moreover, non-specific post-radiotherapeutic changes (e.g., radiation necrosis, gliosis, unspecific blood–brain barrier disturbance) could be differentiated from tumor tissue with a higher accuracy [12-14]. A recent study demonstrated that MET-PET could improve the ability to identify areas with a high risk of local failure in GBM patients [15].

Based on the prior PET studies, we hypothesized that an approach of hypofractionated stereotactic radiotherapy by IMRT (HS-IMRT) with the use of MET-PET data would be an effective strategy for recurrent GBM. This prospective study was designed to measure the acute and late toxicity of patients treated with HS-IMRT planned by MET-PET, response of recurrent GBM to this treatment, overall survival (OS), and the time to disease progression after treatment.

Methods

Patients eligibility

Patients were recruited from September 2007 to August 2011. Adult patients (aged ≥ 18 years) with histopathologic confirmation of GBM who had local recurrent tumor were eligible. Primary treatment consisted of subtotal surgical resection in all patients. All patients had a Karnofsky performance status (KPS) ≥ 60 and were previously treated with external postoperative radiotherapy to a mean and median dose of 60 Gy (range 54 Gy–68 Gy) with concomitant and adjuvant Temozolomide (TMZ) chemotherapy. Additional inclusion criteria consisted of the following: age 18 years or older; first macroscopical relapse at the original site; and adequate bone marrow, hepatic, and renal function. In all cases, a multidisciplinary panel judged the resectability of the lesion before inclusion in this study. Thus patients with non-resectable lesions were included in the study.

Study design

This prospective nonrandomized single-institution study was approved by the Department of Radiation Oncology of Kizawa Memorial Hospital Institutional Review Board. Informed consent was obtained from each subject after disclosing the potential risks of HS-IMRT and discussion of potential alternative treatments. Baseline evaluation included gadolinium-enhanced brain MRI and MET-PET, complete physical and neurological examination, and blood and urine tests within 2 weeks before treatment. After completion of HS-IMRT, patients underwent a physical and neurological examination and a repeat brain MRI and MET-PET. TMZ chemotherapy was continued in a manner consistent with standard clinical use after HS-IMRT course.

Imaging: CT

CT (matrix size: 512 × 512, FOV 50 × 50 cm) was performed using a helical CT instrument (Light Speed; General Electric, Waukesha, WI). The patient head was immobilized in a commercially available stereotactic mask, and scans were performed with a 2.5-mm slice thickness without a gap.

Imaging: MRI

MRI (matrix size: 256 × 256, FOV 25 × 25 cm) for radiation treatment planning was performed using a 1.5-T instrument (Light Speed; General Electric). A standard head coil without rigid immobilization was used. An axial, three-dimensional gradient echo T1-weighted sequence with gadolinium and 2.0-mm slice thickness were acquired from the foramen magnum to the vertex, perpendicular to the main magnetic field.

Imaging: MET-PET

An ADVANCE NXi Imaging System (General Electric Yokokawa Medical System, Hino-shi, Tokyo), which provides 35 transaxial images at 4.25-mm intervals, was used for PET scanning. A crystal width of 4.0 mm (transaxial) was used. The in-plane spatial resolution (full width at half-maximum) was 4.8 mm, and scans were performed in a standard two-dimensional mode. Before emission scans were performed, a 3-min transmission scan was performed to correct photon attenuation using a ring source containing 68Ge. A dose of 7.0 MBq/kg of MET was injected intravenously. Emission scans were acquired for 30 min, beginning 5 min after MET injection. During MET-PET data acquisition, head motion was continuously monitored using laser beams projected onto ink markers drawn over the forehead skin and corrected as necessary. PET/CT and MRI volumes were fused using commercially available software (Syntegra, Philips Medical System, Fitchburg, WI) using a combination of automatic and manual methods. Fusion accuracy was evaluated by a consensus of 3 expert radiologists with 15 years of experience using anatomical fiducials such as the eyeball, lacrimal glands, and lateral ventricles.

Radiation technique

Target volumes were delineated on the registered PET/CT-MRI images and were used to plan HS-IMRT delivery. In this preliminary study, GTV was defined as using an area of high uptake on MET-PET (Figure 1). This high-uptake region was defined using a threshold value for the lesion versus normal tissue counts of radioisotope per pixel index of at least 1.3. A previous study with high-grade gliomas, comparing the exact local MET uptake

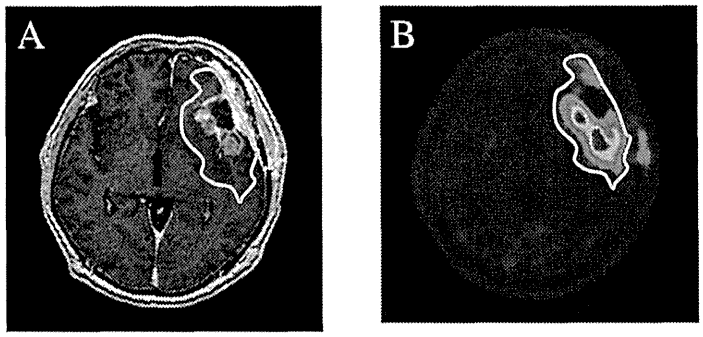

Figure 1 An example of a target planned for a hypofractionated stereotactic radiotherapy using intensity modulated radiation therapy. (A) Contrast-enhanced T1-weighted magnetic resonance imaging. **(B)** ^{11}C-methionine positron emission tomography (MET-PET). Gross tumor volume was defined as the region with high MET uptake (yellow line). The threshold for increased MET uptake was set to ≥1.3 in the contiguous tumor region.

with histology of stereotaxically guided biopsies, demonstrated a sensitivity of 87% and specificity of 89% for the detection of tumor tissue at the same threshold of 1.3-fold MET uptake relative to normal brain tissue [16]. Further, this threshold was validated in a study using diffusion tensor imaging in comparison with MET uptake [17]. Although the delineation of GTV was done by using the automatic contouring mode (Philips Pinnacle v9.0 treatment planning system), the final determination of GTV was confirmed by consensus among 3 observers based on the co-registered MRI and PET data. The PET/MRI fusion image was positioned properly by CT scans equipped with Helical TomoTherapy (TomoTherapy Inc., Madison, WI). Finally, the GTV was expanded uniformly by 3 mm to generate the planning target volume (PTV). The prescribed dose for re-irradiation was based on tumor volume, prior radiation dose, time since external post-operative radiotherapy, and location of the lesion with proximity to eloquent brain or radiosensitive structures. Radiosensitive structures, including the brainstem, optic chiasm, lens, optic nerves, and cerebral cortex, were outlined, and dose-volume histograms for each structure were obtained to ensure that doses delivered to these structures were tolerable. Considering these different conditions, the dose for PTV was prescribed using the 80-95% isodose line, and the total doses were arranged from 25 Gy to 35 Gy in each patient. The dose maps and dose-volume histograms of a representative case are illustrated in Figure 2.

Chemotherapy

After HS-IMRT course, a dose of 200 mg/m^2/day for 5 days with TMZ chemotherapy was administered. Cycles were repeated every 28 days with 3 or more cycles after HS-IMRT. Treatment was discontinued when unequivocal progression or severe toxicity occurred. TMZ was not administrated in patients who refused treatment or did not meet inclusion criteria. Patient inclusion criteria for TMZ chemotherapy consisted of the following: KPS score 50 or higher; evidence of good maintenance of major organ function (bone marrow, liver, kidney, etc.) in routine laboratory studies; expected to survive more than 3 months.

Follow-up

Regular serial neurological and radiological examinations were initially performed at 1 month after completion of treatment and then every 2 months thereafter or in the event of neurological decay. Follow-up examinations included MRI and MET-PET imaging. If the MRI revealed further enlargement of the enhanced mass, the lesion was diagnosed as "local progression", and the day on which MRI first revealed lesion enlargement was defined as the date of progression. However, in cases with low MET uptake on PET in the MRI-enhanced lesion, the diagnosis was changed to "radiation necrosis". The criterion of MET-PET differential diagnosis between local progression and radiation necrosis was utilized in a previous MET-PET study by Takenaka et al. [18]. However, all patients couldn't be applied with PET examination in the follow up study. In cases without PET examination, diagnosis of radiation necrosis was based on pathologic examination or clinical course. Cases in which lesions showed spontaneous shrinkage or decreased in size during corticosteroid treatment were also defined as "radiation necrosis". A diagnosis of "distant failure" was defined as the appearance of a new enhanced lesion distant from the original tumor site. Either local progression or distant failure was defined as disease progression. Acute and late toxicities were determined based on the Common Terminology Criteria for Advance Events (version 4).

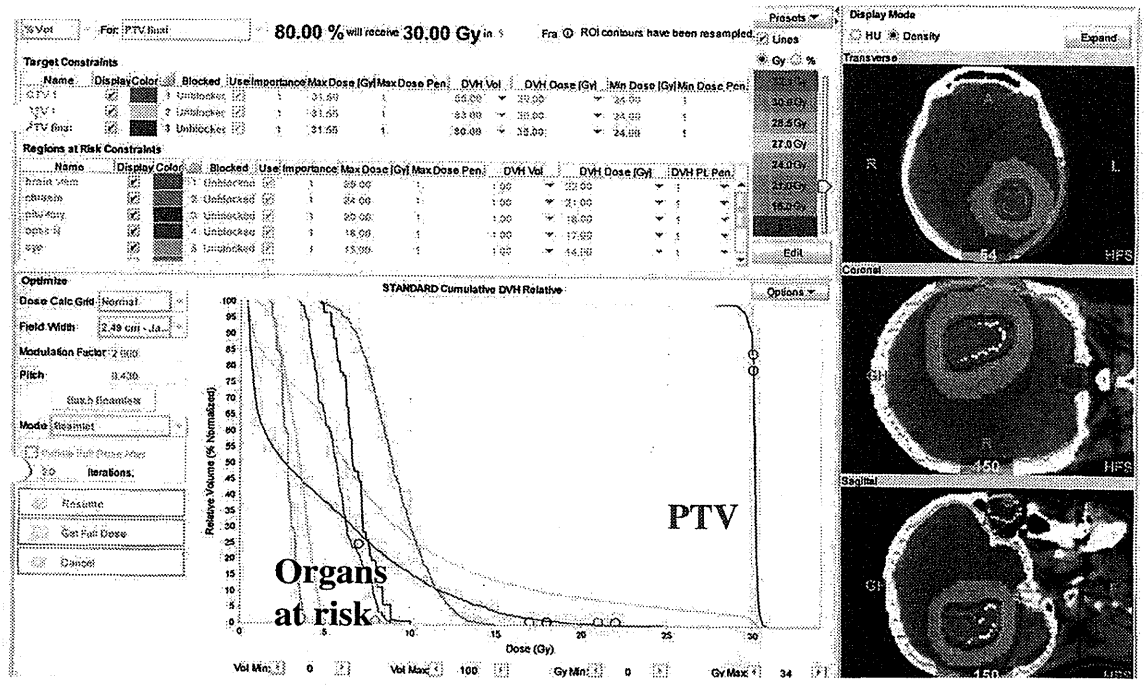

Figure 2 A dose map and dose-volume histogram of a representative case. Prescribed dose for planning target volume (PTV) and the doses of organs at risk were demonstrated.

Statistical analysis

Survival events were defined as death from any cause for OS and as disease progression for progression-free survival (PFS). OS and PFS were analyzed from the date of HS-IMRT to the date of the documented event using the Kaplan-Meier method. Tumor- and therapy-related variables were tested for a possible correlation with survival, using the Log-rank test. Variables included age (≥50 vs. <50), KPS (≥70 vs. <70), and combined TMZ chemotherapy ("yes" vs. "no"). P-values of less than 0.05 were considered significant. Prognostic factors were further evaluated in a multivariate stepwise Cox regression analysis.

Results

Twenty-one patients (18 men, 3 women) with histologically confirmed GBM were enrolled in this trial (Table 1). The median patient age was 53.9 years (range 22–76), and median KPS was 80 (range 60–90).

The median elapsed time between external postoperative radiotherapy and study enrollment was 12 months (range, 3–48 months). HS-IMRT was performed in 5 fractions, keeping a total dose for the PTV at 25 Gy in 6 patients, 30 Gy in 11 patients, and 35 Gy in 4 patients, given as 5- to 7-Gy daily over a period of 5 days. The average PTV was 27.4 ± 24.1 cm^3 (3.4 - 102.9 cm^3). All 21 patients completed the prescribed HS-IMRT course. Overall, thirteen patients (62%) received combined modality treatment with TMZ.

Toxicity assessment

No patients demonstrated significant acute toxicity, and all patients were able to complete the prescribed radiation dose without interruption. In the late phase, Grade

Table 1 Patient characteristics

Parameter	n (%)
Age, years	
≥50	13 (62)
<50	8 (38)
Gender	
Male	18 (86)
Female	3 (14)
KPS score	
≥70	16 (76)
<70	5 (24)
Combined TMZ chemotherapy	
Yes	13 (62)
No	8 (38)

Abbreviations: KPS Karnofsky performance status, *TMZ* temozolomide.

2 radiation necrosis was observed in 1 patient, although the lesion was decreased in size during corticosteroid treatment. One patient who received a dose of radiation of 25.0 Gy, experienced Grade 4 radiation necrosis in the form of mental deterioration 4 months after HS-IMRT. In this case, a second necrotomy was required 5 months after HS-IMRT. Although after a second surgery, the patient's clinical condition was stable for a long period, disease progression occurred 40 months after HS-IMRT, causing death. The actuarial reoperation rate was 4.8% for radiation necrosis.

Outcomes

With a median follow-up of 12 months, the median OS was 11 months from the date of HS-IMRT, with a 6-month and 1-year survival rate of 71.4% and 38.1%, respectively (Figure 3A). The survival rates by age, KPS, and TMZ chemotherapy are shown in Figure 4A-C. OS of patients with KPS 70 or over was 12 months versus 5 months for patients with KPS less than 70. KPS was a significant prognostic factor of OS as tested by univariate analysis ($p < 0.001$). OS of patients who received combined TMZ chemotherapy was 12 months versus 6 months for patients who did not receive chemotherapy. The differences between the two groups approached significance ($p = 0.079$). In the multivariate model, only KPS remained statistically significant ($p = 0.005$) (Table 2).

The median PFS was 6 months from the date of HS-IMRT treatment, with a 6-month and 1-year survival rate of 38.1% and 14.3%, respectively (Figure 3B). KPS was the significant prognostic factor for PFS as tested by univariate analysis ($p = 0.016$). On multivariate analysis, none of the variables were significantly predictive of PFS (Table 3).

A representative case is shown in Figure 5, in which a follow-up MET-PET scan was performed to improve the diagnostic accuracy.

Discussion

Recently, much work has been performed on various fractionation regimens and dose escalation with IMRT for GBM. These studies reveal relatively favorable survival results [1-4], although a distinct advantage over conventional radiation therapy has not been demonstrated. However, if a precise conformal treatment technique such as HS-IMRT is utilized, and a greater biologic dose to the infiltrating tumor is achieved through hypo-fractionation, it

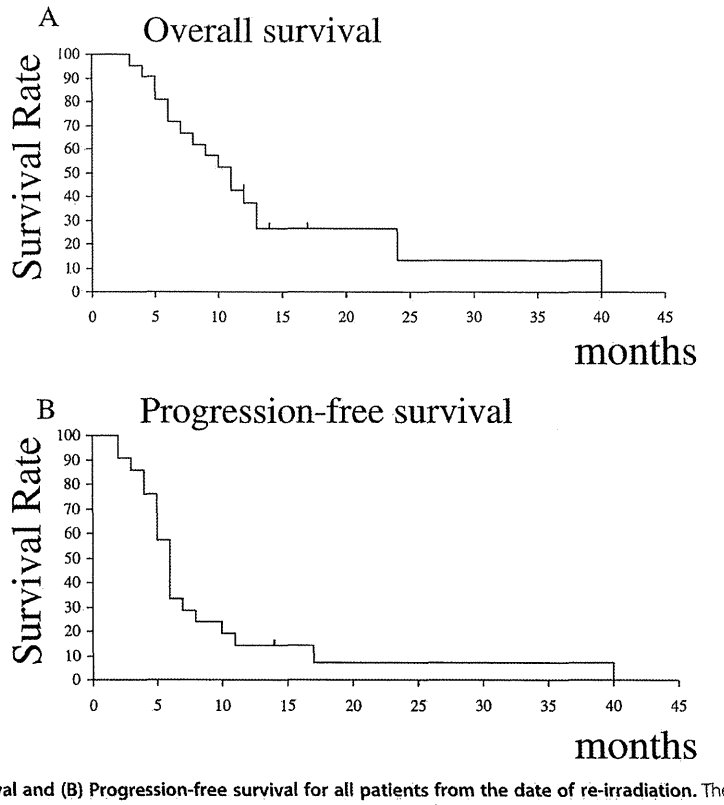

Figure 3 (A) Overall survival and (B) Progression-free survival for all patients from the date of re-irradiation. The median overall survival time was 11 months, and the median progression-free survival time was 6 months from the date of re-irradiation, respectively.

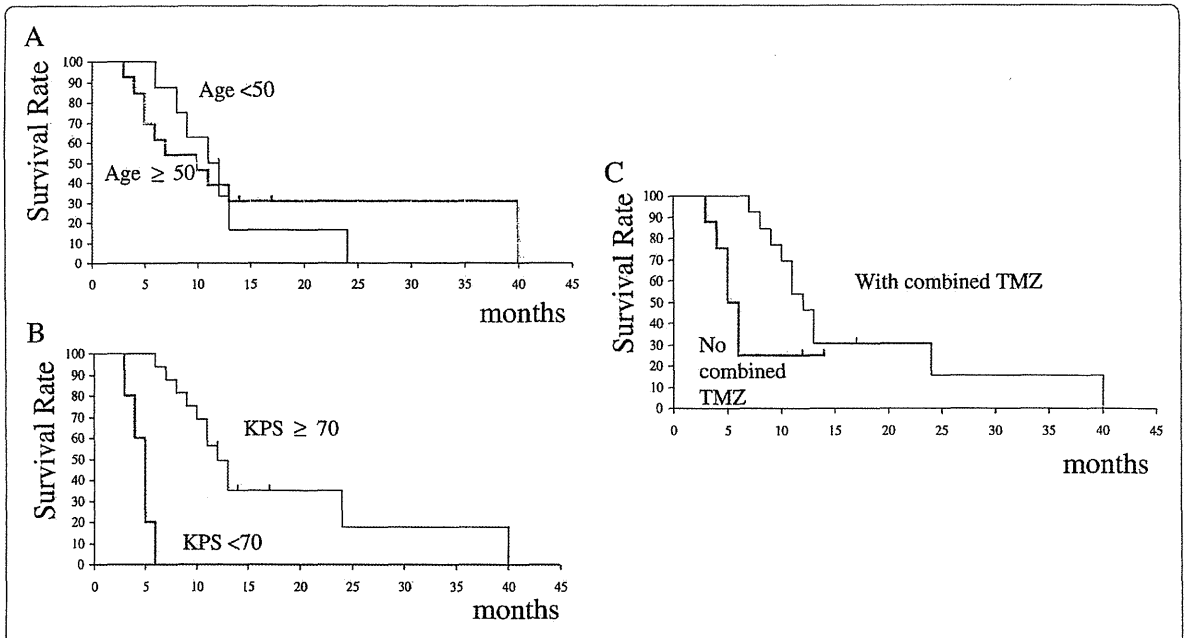

Figure 4 Overall survival rates among different subgroups by (A) age, (B) Karnofsky performance status (KPS), and (C) combined temozolomide (TMZ) chemotherapy.

could be possible to deliver an effective therapy that may increase patient survival without increasing morbidity. To meet these requirements, the contouring of the target volume is of critical importance.

PET is a newer imaging method that can improve the visualization of biological processes. In recent PET studies, analysis of the metabolic and histologic characteristics provided evidence that regional high MET uptake correlates with the malignant pathologic features [6-8,16]. Furthermore, nonspecific post-therapeutic changes could be differentiated from tumor tissue with a higher accuracy [12-14]. These findings support the notion that complementary information derived from MET uptake may be helpful in developing individualized, patient-tailored therapy strategies in patients with recurrent GBM.

This prospective study was designed to measure the acute and late toxicity of patients treated with HS-IMRT planned by MET-PET, response of recurrent GBM to

Table 2 Analysis of prognostic variables for overall survival

Variables	Median survival (months)	Univariate analysis* *p* value	Multivariate analysis† *p* value
Age			
≥50	10	0.931	
<50	11		
KPS			
≥70	12	<0.001	0.005
<70	5		
Combined TMZ chemotherapy			
Yes	12	0.079	0.581
No	6		

Abbreviations as in Table 1.
Statistical analyses were performed with *Log - rank test and †Cox's proportional hazards model.

Table 3 Analysis of prognostic variables for progression - free survival

Variables	Median survival (months)	Univariate analysis* *p* value	Multivariate analysis† *p* value
Age			
≥50	6	0.279	
<50	6		
KPS			
≥70	6	0.016	0.059
<70	5		
Combined TMZ chemotherapy			
Yes	6	0.447	0.479
No	5		

Abbreviations as in Table 1.
Statistical analyses were performed with *Log - rank test and †Cox's proportional hazards model.

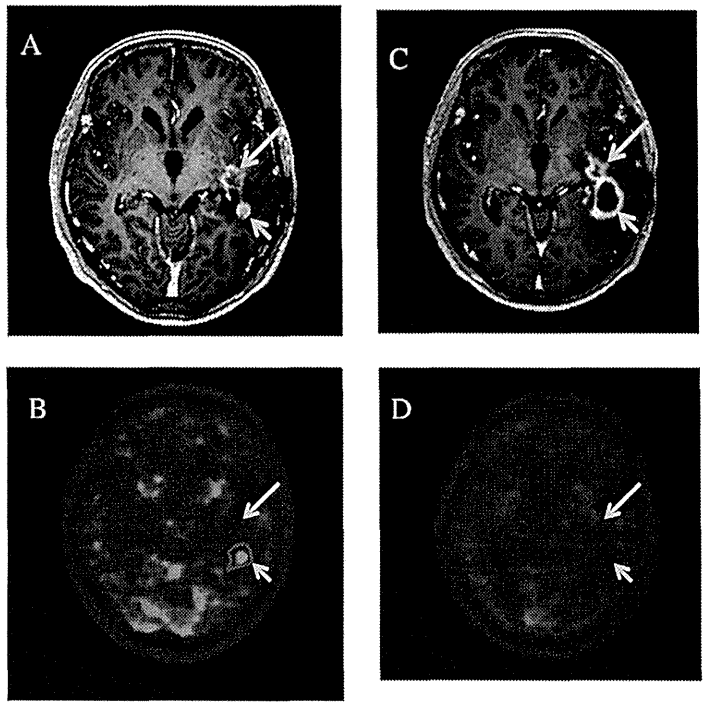

Figure 5 Recurrent glioblastoma multiforme (GBM) in a 55-year-old man before and after hypofractionated stereotactic radiotherapy by intensity modulated radiation therapy (HS-IMRT). Before HS-IMRT, two enhanced lesions (long and short arrow) were demonstrated in the left temporal lobe on T1-weighted magnetic resonance imaging **(A)**. ^{11}C-methionine positron emission tomography (MET-PET) demonstrated a MET high-uptake on the region of short arrow, which was defined as the Gross Tumor Volume (red line) **(B)**. 5 months after HS-IMRT, there was no tumor recurrence on the lesion (long arrow, **C** & **D**). The enhanced lesion (short arrow) was increased in size **(C)**, although MET uptake decreased relative to normal tissue, which suggested a necrotic change in the irradiated region **(D)**. The patient had no neurologic deficits or quality of life issues. KPS was 90%.

this treatment, OS, and the time to disease progression after treatment. We found that the OS rate from re-irradiation was 11 months and that the 6-month and 1-year OS rates were 71.4% and 38.1%, respectively (Figure 3). The survival results of our study appeared to be favorable compared to prior studies using other hypofractionated stereotactic radiotherapy in recurrent malignant glioma [19-22]. Also, we observed an improved toxicity profile, suggesting that hypofractionated stereotactic radiotherapy should be considered standard salvage therapy for previously irradiated high-grade gliomas [23]. We hypothesized that MET-PET/CT/MRI image fusion could facilitate target volume delineation and normal tissue sparing. This might lead to an improved therapeutic ratio, especially in pre-treated patients, in which post-therapy changes in CT or MRI, as with contrast enhancement, are difficult to distinguish from tumor recurrence (Figure 5).

In our study, KPS ≥ 70% was associated with longer patient survival, as previously described for recurrent GBM [21]. In addition, we observed a trend toward a beneficial effect on OS when combining TMZ chemotherapy (Figure 4C, Table 2). We estimated that the addition of TMZ might be particularly effective if the radiation dose to normal brain tissue was limited by better targeting. However, the impact of TMZ along with the methylation status of the O-6-methylguanine-DNA methyltransferase (MGMT) on survival was not systematically evaluated in the present study. This study has a selection bias which necessitates prospective studies, as the patients with methylated MGMT or who were in better clinical condition were more likely to have received adjuvant TMZ chemotherapy. Nevertheless, the results of this study support our initial work and further establish the efficacy of this HS-IMRT regimen combined with TMZ.

Both single-fraction stereotactic radiosurgery and brachytherapy have been reported to have modest utility as palliative salvage interventions; however, both have been associated with high rates of re-operation because of the associated toxicity [24,25]. Our initial experience with HS-IMRT used the 5- to 7-Gy fractions to a maximum of 35 Gy and reported an actuarial reoperation rate of 4.8% for radiation necrosis, providing additional support that

this dose and fraction size is well tolerated. In our opinion, MET-PET/CT/MR image fusion could facilitate target volume delineation and normal tissue sparing, which might lead to an improved therapeutic ratio. MET-PET/CT/MR image fusion planning, which examines biological behavior in re-irradiation, seems not only to decrease the likelihood of geographical misses in target volume definition, but also to facilitate normal tissue sparing and toxicity reduction, especially when conformal treatment technique such as HS-IMRT is implemented.

Conclusions

This is the first prospective study using biologic imaging to optimize HS-IMRT using MET-PET/CT/MRI image fusion in recurrent GBM. A low frequency of side effects was observed. HS-IMRT with PET data seems to be well tolerated and resulted in a median survival time of 11 months after HS-IMRT, although a properly designed randomized trial are necessary to firmly establish whether the present regimen is superior to the other treatment methods for recurrent GBM.

Competing interest

The authors report no competing interest concerning the materials or methods used in this study or the findings specified in this paper.

Authors' contribution

MM and SO carried out the statistical analysis, JS and KY participated in the sequence alignment, and JY, HY, and TI drafted the manuscript. All authors read and approved the final manuscript.

Author details

[1]Chubu Medical Center for Prolonged Traumatic Brain Dysfunction, Kizawa Memorial Hospital, Minokamo, Gifu, Japan. [2]Department of Radiation Oncology, Kizawa Memorial Hospital, Minokamo, Gifu, Japan. [3]Department of Neurosurgery, Kizawa Memorial Hospital, Minokamo, Gifu, Japan. [4]Department of Neurosurgery, Gifu University Graduate School of Medicine, Gifu, Japan. [5]Department of Neurosurgery, Chubu Medical Center for Prolonged Traumatic Brain Dysfunction, 630 Shimokobi, Kobi-cho, Minokamo, Gifu 505-0034, Japan.

Received: 23 April 2014 Accepted: 12 August 2014
Published: 14 August 2014

References

1. Iuchi T, Hatano K, Narita Y, Kodama T, Yamaki T, Osato K: **Hypofractionated high-dose irradiation for the treatment of malignant astrocytomas using simultaneous integrated boost technique by IMRT.** *Int J Radiat Oncol Biol Phys* 2006, **64**:1317–1324.
2. Sultanem K, Patrocinio H, Lambert C, Corns R, Leblanc R, Parker W, Shenouda G, Souhami L: **The use of hypofractionated intensity-modulated irradiation in the treatment of glioblastoma multiforme: preliminary results of a prospective trial.** *Int J Radiat Oncol Biol Phys* 2004, **58**:247–252.
3. Floyd NS, Woo SY, The BS, Prado C, Mai WY, Trask T, Gildenberg PL, Holoye P, Augspurger ME, Carpenter LS, Lu HH, Chiu JK, Grant WH 3rd, Butler EB: **Hypofractionated intensity-modulated radiotherapy for primary glioblastoma multiforme.** *Int J Radiat Oncol Biol Phys* 2004, **58**:721–726.
4. Panet-Raymond V, Souhami L, Roberge D, Kavan P, Shakibnia L, Muanza T, Lambert C, Leblanc R, Del Maestro R, Guiot MC, Shenouda G: **Accelerated hypofractionated intensity-modulated radiotherapy with concurrent and adjuvant temozolomide for patients with glioblastoma multiforme: a safety and efficacy analysis.** *Int J Radiat Oncol Biol Phys* 2009, **73**:473–478.
5. Grosu AL, Weber WA, Franz M, Stärk S, Piert M, Thamm R, Gumprecht H, Schwaiger M, Molls M, Nieder C: **Reirradiation of recurrent high-grade gliomas using amino acid PET (SPECT)/CT/MRI image fusion to determine gross tumor volume for stereotactic fractionated radiotherapy.** *Int J Radiat Oncol Biol Phys* 2005, **63**:511–519.
6. Pirotte B, Goldman S, Dewitte O, Massager N, Wikler D, Lefranc F, Ben Taib NO, Rorive S, David P, Brotchi J, Levivier M: **Integrated positron emission tomography and magnetic resonance imaging-guided resection of brain tumors: a report of 103 consecutive procedures.** *J Neurosurg* 2006, **104**:238–253.
7. Mosskin M, Ericson K, Hindmarsh T, von Holst H, Collins VP, Bergström M, Eriksson L, Johnström P: **Positron emission tomography compared with magnetic resonance imaging and computed tomography in supratentorial gliomas using multiple stereotactic biopsies as reference.** *Acta Radiol* 1989, **30**:225–232.
8. Ogawa T, Shishido F, Kanno I, Inugami A, Fujita H, Murakami M, Shimosegawa E, Ito H, Hatazawa J, Okudera T: **Cerebral glioma: evaluation with methionine PET.** *Radiology* 1993, **186**:45–53.
9. Miwa K, Shinoda J, Yano H, Okumura A, Iwama T, Nakashima T, Sakai N: **Discrepancy between lesion distributions on methionine PET and MR images in patients with glioblastoma multiforme: insight from a PET and MR fusion image study.** *J Neurol Neurosurg Psychiatry* 2004, **75**:1457–1462.
10. Matsuo M, Miwa K, Tanaka O, Shinoda J, Nishibori H, Tsuge Y, Yano H, Iwama T, Hayashi S, Hoshi H, Yamada J, Kanematsu M, Aoyama H: **Impact of [(11)C] Methionine positron emission tomography for target definition of glioblastoma multiforme in radiation therapy planning.** *Int J Radiat Oncol Biol Phys* 2012, **2012**(82):83–89.
11. Miwa K, Matsuo M, Shinoda J, Oka N, Kato T, Okumura A, Ueda T, Yokoyama K, Yamada J, Yano H, Yoshimura S, Iwama T: **Simultaneous integrated boost technique by helical tomotherapy for the treatment of glioblastoma multiforme with 11C-methionine PET: report of three cases.** *J Neurooncol* 2008, **87**:333–339.
12. Terakawa Y, Tsuyuguchi N, Iwai Y, Yamanaka K, Higashiyama S, Takami T, Ohata K: **Diagnostic accuracy of 11C-methionine PET for differentiation of recurrent brain tumors from radiation necrosis after radiotherapy.** *J Nucl Med* 2008, **49**:694–699.
13. Grosu AL, Lachner R, Wiedenmann N, Stärk S, Thamm R, Kneschaurek P, Schwaiger M, Molls M, Weber WA: **Validation of a method for automatic image fusion (BrainLAB system) of CT data and 11C-methionine PET data for stereotactic radiotherapy using a LINAC: first clinical experience.** *Int J Radiat Oncol Biol Phys* 2003, **56**:1450–1463.
14. Grosu AL, Weber WA, Riedel E, Jeremic B, Nieder C, Franz M, Gumprecht H, Jaeger R, Schwaiger M, Molls M: **L-(methyl-11C) methionine positron emissions tomography for target delineation in resected high grade gliomas before radiation therapy.** *Int J Radiat Oncol Biol Phys* 2005, **63**:64–74.
15. Lee IH, Piert M, Gomez-Hassan D, Junck L, Rogers L, Hayman J, Ten Haken RK, Lawrence TS, Cao Y, Tsien C: **Association of 11C-methionine PET uptake with site of failure after concurrent temozolomide and radiation for primary glioblastoma multiforme.** *Int J Radiat Oncol Biol Phys* 2009, **73**:479–485.
16. Kracht LW, Miletic H, Busch S, Jacobs AH, Voges J, Hoevels M, Klein JC, Herholz K, Heiss WD: **Delineation of brain tumor extent with [11C] L-methionine positron emission tomography: local comparison with stereotactic histopathology.** *Clin Cancer Res* 2004, **10**:7163–7170.
17. Kinoshita M, Hashimoto N, Goto T, Yanagisawa T, Okita Y, Kagawa N, Kishima H, Tanaka H, Fujita N, Shimosegawa E, Hatazawa J, Yoshimine T: **Use of fractional anisotropy for determination of the cut-off value in 11C-methionine positron emission tomography for glioma.** *Neuroimage* 2009, **45**:312–318.
18. Takenaka S, Asano Y, Shinoda J, Nomura Y, Yonezawa S, Miwa K, Yano H, Iwama T: **Comparison of 11C-methionine, 11C-choline, and 18F-fluorodeoxyglucose-PET for distinguishing glioma recurrence from radiation necrosis.** *Neurol Med Chir (Tokyo)* 2014, **54**:280–289.
19. Combs SE, Thilmann C, Edler L, Debus J, Schulz-Ertner D: **Efficacy of fractionated stereotactic reirradiation in recurrent gliomas: long-term result in 172 patients treated in a single institution.** *J Clin Oncol* 2005, **23**:8863–8869.
20. Ernst-Stecken A, Ganslandt O, Lambrecht U, Sauer R, Grabenbauer G: **Survival and quality of life after hypofractionatedstereotactic radiotherapy for recurrent malignant glioma.** *J Neurooncol* 2007, **81**:287–294.
21. Fokas E, Wacker U, Gross MW, Henzel M, Encheva E, Engenhart-Cabillic R: **Hypofractionated stereotactic reirradiation of recurrent glioblastomas:**

a beneficial treatment option after high-dose radiotherapy? *Strahlenther Onkol* 2009, 185:235–240.
22. Henke G, Paulsen F, Steinbach JP, Ganswindt U, Isijanov H, Kortmann RD, Bamberg M, Belka C: Hypofractionated reirradiation for recurrent malignant glioma. *Strahlenther Onkol* 2009, 185:113–119.
23. Fogh SE, Andrews DW, Glass J, Curran W, Glass C, Champ C, Evans JJ, Hyslop T, Pequignot E, Downes B, Comber E, Maltenfort M, Dicker AP, Werner-Wasik M: Hypofractionated stereotactic radiation therapy: an effective therapy for recurrent high-grade gliomas. *J Clin Oncol* 2010, 28:3048–3053.
24. Gutin PH, Prados MD, Phillips TL, Wara WM, Larson DA, Leibel SA, Sneed PK, Levin VA, Weaver KA, Silver P: External irradiation followed by an interstitial high activity iodine-125 implant "boost" in the initial treatment of malignant gliomas: NCOG study 6G-82-2. *Int J Radiat Oncol Biol Phys* 1991, 21:601–606.
25. Hall WA, Djalilian HR, Sperduto PW, Cho KH, Gerbi BJ, Gibbons JP, Rohr M, Clark HB: Stereotactic radiosurgery for recurrent malignant gliomas. *J Clin Oncol* 1995, 13:1642–1648.

doi:10.1186/1748-717X-9-181
Cite this article as: Miwa *et al.*: Re-irradiation of recurrent glioblastoma multiforme using ^{11}C-methionine PET/CT/MRI image fusion for hypofractionated stereotactic radiotherapy by intensity modulated radiation therapy. *Radiation Oncology* 2014 9:181.

J Neurooncol
DOI 10.1007/s11060-014-1453-y

CLINICAL STUDY

Bevacizumab treatment leads to observable morphological and metabolic changes in brain radiation necrosis

Shingo Yonezawa · Kazuhiro Miwa · Jun Shinoda · Yuichi Nomura · Yoshitaka Asano · Noriyuki Nakayama · Naoyuki Ohe · Hirohito Yano · Toru Iwama

Received: 7 January 2014 / Accepted: 20 April 2014

Abstract We investigated morphological and metabolic changes of radiation necrosis (RN) of the brain following bevacizumab (BEV) treatment by using neuroimaging. Nine patients with symptomatic RN, who had already been treated with radiation therapy for malignant brain tumors (6 glioblastomas, 1 anaplastic oligodendroglioma, and 2 metastatic brain tumors), were enrolled in this prospective clinical study. RN diagnosis was neuroradiologically determined with Gd-enhanced MRI and 11C-methionine positron emission tomography (MET-PET). RN clinical and radiological changes in MRI, magnetic resonance spectroscopy (MRS) and PET were assessed following BEV therapy. Karnofsky performance status scores improved in seven patients (77.8 %). Both volumes of the Gd-enhanced area and FLAIR-high area from MRI decreased in all patients after BEV therapy and the mean size reduction rates of the lesions were 80.0 and 65.0 %, respectively. MRS, which was performed in three patients, showed a significant reduction in Cho/Cr ratio after BEV therapy. Lesion/normal tissue (L/N) ratios in MET- and 11C-choline positron emission tomography (CHO-PET) decreased in 8 (89 %) and 9 patients (100 %), respectively, and the mean L/N ratio reduction rates were 24.4 and 60.7 %, respectively. BEV-related adverse effects of grade 1 or 2 (anemia, neutropenia and lymphocytopenia) occurred in three patients. These results demonstrated that BEV therapy improved RN both clinically and radiologically. BEV therapeutic mechanisms on RN have been suggested to be related not only to the effect on vascular permeability reduction by repairing the blood–brain barrier, but also to the effect on suppression of tissue biological activity, such as immunoreactions and inflammation.

Keywords Bevacizumab · Radiation necrosis · Positron emission tomography · Magnetic resonance imaging · Magnetic resonance spectroscopy

S. Yonezawa (✉) · K. Miwa · J. Shinoda · Y. Nomura · Y. Asano
Chubu Medical Center for Prolonged Traumatic Brain Dysfunction, Kizawa Memorial Hospital, 630 Shimokobi, Kobi-cho, Minokamo, Gifu 505-0034, Japan
e-mail: syonezawa0712@gmail.com

S. Yonezawa · K. Miwa · J. Shinoda · Y. Nomura · Y. Asano
Department of Clinical Brain Sciences, Gifu University Graduate School of Medicine, Minokamo, Japan

S. Yonezawa · Y. Nomura · N. Nakayama · N. Ohe · H. Yano · T. Iwama
Department of Neurosurgery, Gifu University Graduate School of Medicine, Gifu, Japan

Introduction

Radiotherapy plays an important role among multidisciplinary therapies for malignant brain tumors and contributes to extension of survival time. However, radiation necrosis (RN), which is a late effect after radiation therapy for brain tumors, is still one of the most critical pathologies in the neuro-oncology clinic. More importantly, the risk of RN may increase with propagation of high power modalities for radiation therapy. RN often represents symptomatic disorders with general and neurological deterioration and sometimes leads to mortal conditions because of intensive brain edema around the growing necrotic core.

Currently, the best non-surgical treatment for RN is hyperbaric oxygen therapy or combination therapies using steroids, anti-coagulants, and vitamin E; however, the resulting clinical effects are minimal [1, 2]. Surgical removal of the necrotic lesion is another treatment that

Published online: 01 May 2014

controls intensive brain edema as well as simultaneously examines for the presence of tumor recurrence. However, there are therapeutic limitations of RN surgical removal in cases of lesions in unresectable areas [3].

Strongly related to tumor progression, vascular endothelial growth factor (VEGF) has been thought to play a major part in angiogenesis, i.e., VEGF can facilitate proliferation and migration of vascular endothelial cells and increase vascular permeability. Bevacizumab (BEV) is a molecular-target medicine using a humanized murine monoclonal antibody that can selectively inhibit VEGF biological effects and has been clinically used in treatment of various solid tumors, inhibiting tumor angiogenesis [4]. In addition, VEGF is responsible for factors related to RN deep growth. Nordal et al. [5] have reported that VEGF knockout mice are resistant to radiation injury. Nonoguchi et al. [6] suggested that VEGF-producing astrocytes concentrated in perinecrotic areas might be a universal cause of pathological angiogenesis in RN and subsequent perilesional edema. Therefore, BEV has been expected to be a promising new agent for RN treatment.

Potential beneficial effects of BEV treatment on RN were first reported by Gonzalez et al. [7] in their retrospective clinical analysis in 2007. This study was followed by a 2011 randomized double-blind placebo-controlled trial of BEV therapy for RN by Levin et al. [8]. They reported that all BEV-treated patients demonstrated decreases in necrosis volumes estimated by both FLAIR and T1-weighted Gd-enhanced MRI [7, 8]. Clinical improvement in RN patients by BEV treatment has also been shown in other reports [7–10].

To our knowledge, there have been no reports on the metabolic evaluation of BEV effects on RN. Thus, in the present study, for the first time, we report both morphological and metabolic changes of RN following BEV treatment using MRI, proton magnetic resonance spectroscopy (MRS), 11C-methionine positron emission tomography (MET-PET), and 11C-choline positron emission tomography (CHO-PET). In addition, clinical effects and adverse events of BEV treatment are described.

Methods

Patient population

Nine symptomatic cerebral RN patients aged 37–64 years (average: 52.8 years), who had already been treated with radiation therapy for their malignant brain tumors (6 glioblastomas (GBM), 1 anaplastic oligodendroglioma, and 2 metastatic brain tumors), with neither clinical nor radiological improvement upon medical treatment with steroids, were enrolled in the clinical pilot study using BEV against RN at Kizawa Memorial Hospital between June 2010 and September 2011. Radiological RN was diagnosed based on neuroimaging criteria described below (in "Diagnosis of RN" section). This prospective nonrandomized single-institution study was approved by the local ethics committee of Kizawa Memorial Hospital. Each patient provided written informed consent prior to treatment and inclusion in this study. All patient characteristics are shown in Table 1. All 6 GBM patients were treated by hypofractionated radiotherapy according to our institutional protocol [11, 12].

Patient eligibility criteria for study enrollment consisted of the following: receipt of cranial irradiation for brain neoplasm or neoplasm adjacent to brain or head and neck cancer; diagnosed with RN by MET-PET; developed symptoms due to the necrotic lesion; Karnofsky performance status (KPS) score 60 or higher; no evidence of symptom improvement by conventional medical treatment; difficulty or high risk in necrotic lesion removal; evidence of good maintenance of major organ function (bone marrow, liver, kidney, etc.) in routine laboratory studies; expected to survive more than 3 months; able to understand and willing to sign a written informed consent document.

Exclusion criteria for this study included the following: prominent infection; high fever (>100.4 °F); clinically significant complications such as cardiovascular disease, pulmonary fibrous, interstitial pneumonia, bleeding tendency, uncontrollable hypertension or diabetes mellitus at the time of study; active bleeding (such as intracranial, gastrointestinal, urinary, retroperitoneal, pulmonary, tracheo-bronchial hemorrhage); severe BEV hypersensitivity; pregnancy or lactation or the willingness and expectation to become pregnant; and judged to be inappropriate for the study by the medical attendant.

BEV therapy

All 9 patients were treated using BEV intravenously with a dose of 5 mg/kg biweekly (one cycle), for a total dose of 30 mg/kg (6 cycles).

MRI

MRI was performed with a 3.0 T system (Achieva; Philips Medical Systems, Milwaukee, WI). Axial T1-weighted images (TR/TE/NEX = 350/9/2) and T2-weighted images (2300/100/2) (FOV 24 × 24-cm, matrix size 512 × 256) were acquired. The slice thickness was 6 mm, with a 3-mm slice gap. For co-registration of metabolic and anatomic data, 3D spoiled gradient-echo images were also acquired after administration of 0.2 ml/kg of gadolinium (Gd) (Gd-DTPA, Magnevist; Nihon Shering, Osaka, Japan) (Gd-MRI) using

Table 1 Clinical features of RN patients

Case no.	Age	Sex	Primary tumor pathology	RT (Gy)	Interval after RT (months)	Symptoms	Survival after BEV therapy (months)
1	45	M	GBM	68(GTV1[111])/8Fr	15	Seizure, aphasia, motor weakness	12 (alive)
2	37	F	GBM	68(GTV1[111])/8Fr	12	Motor weakness	35 (alive)
3	58	M	GBM	68(GTV1[111])/8Fr	25	Motor weakness, headache	19
4	55	M	GBM	68(GTV1[111])/8Fr	6	Headache	18 (alive)
5	57	M	GBM	68(GTV1[111])/8Fr	15	Motor weakness	12
6	54	M	META (lung)	30(WB) + 20(SRS)	15	Seizure, motor weakness	10
7	51	F	META (lung)	30(SRT)/5Fr	23	Headache, numbness	23 (alive)
8	54	M	AO	60(EL) + 25(SRT)/5Fr	13	Seizure, motor weakness	20
9	64	M	GBM	68(GTV1[111])/8Fr	3	Disorientation, motor weakness	14

RN radiation necrosis, *GBM* glioblastoma, *META* metastatic brain tumor, *AO* anaplastic oligodendroglioma, *RT* radiation therapy, *GTV* gross tumor volume, *Fr* fraction, *SRS* stereotactic radiosurgery, *SRT* stereotactic radiotherapy, *WB* whole brain, *EL* extended local, *BEV* bevacizmab

the following parameters: no gap; 1.0-mm thickness; TR/TE = 20.0/1.6 ms; flip angle = 15°; NEX = 1; and axial views.

The volume of Gd-enhanced area on T1-weighted MRI (Gd-volume) and that of the abnormal hyperintense area on fluid attenuated inversion recovery (FLAIR) (FLAIR-volume) before and after BEV therapy were measured in each case using an image analysis program in combination with Dr. View/Linux image analysis software (INFOCOM CORPORATION, Tokyo, Japan). On each axial MRI slice, those areas were manually outlined, measured and summed across slices. These sums were multiplied by the slice interval. The size reduction rates of the Gd-volume and FLAIR-volume were calculated by the formulas below.

Size reduction rate of Gd - volume
= (Gd - volume before BEV therapy
− Gd - volume after BEV therapy)
/Gd - volume before BEV therapy

Size reduction rate of FLAIR - volume
= (FLAIR - volume before BEV therapy
− FLAIR - volume after BEV therapy)
/FLAIR - volume before BEV therapy

MRS

Proton MRS was performed in all 9 patients with the same 3.0-T system using an 8-channel SENSE head coil as mentioned above. Following conventional MRI, but prior to contrast administration, MRSI data were acquired using two dimensional point-resolved spectroscopy (2D-PRESS) slice-selective spin echo sequence with automatic shimming and Gaussian water suppression. Measurement parameters were 2000/288 ms (TR/TE), 23 × 19 cm field of view (FOV), 23 × 18 phase encoding steps, and 8 mm section thickness. The T2-weighted images were used as scout images for the placement of the rectangular volume of interest (VOI) for MRSI acquisition, which extended beyond the suspected RN (hyperintense areas on T2-weighted images) to include normal appearing brain tissue, allowing recording of control spectra. To prevent strong contribution to the spectra from subcutaneous fat signals, the VOI was completely enclosed within the brain. The metabolite peaks were assigned as choline (Cho) at 3.22 ppm and creatine (Cr) at 3.02 ppm. Spectroscopic data were processed on an independent Philips workstation by SpectroView. For multi-voxel MRS analysis, Cho/Cr ratios of each of the 9 voxels in the RN lesions before and after BEV therapy were measured in 3 patients (Cases 2, 7 and 9) in which reliably analyzable spectroscopic data without any remarkable baseline inconsistency could be obtained.

PET

PET was carried out according to standardized procedures recommended by the Japan Radioisotope Association. The PET scanner was an ADVANCE NXi Imaging System (General Electric Yokokawa Medical System, Hino-shi, Tokyo, Japan), which provided 35 transaxial images at 4.25-mm intervals covering a 25.6-cm in-plane field of view. The in-plane spatial resolution (full width at half maximum) was 4.8 mm, and the scan mode was the standard 2D mode. Before the emission scan was performed, a 3 min transmission scan was performed to correct photon attenuation with a ring source containing ^{68}Ge. Patients had fasted for at least 4 h before PET. A venous cannula was inserted into the forearm for radiopharmaceutical

injections. From this cannula, blood samples could also be collected if necessary. A dose of 5.0 MBq/kg of MET or 5.0 MBq/kg of CHO was injected intravenously, depending on the particular examination. Emission scans were acquired for 30 min, beginning 5 min after MET injection; and for 7 min, beginning 2 min after CHO injection. During PET data acquisition, head motion was continuously monitored using laser beams projected onto ink marks drawn on the forehead and was corrected manually, as necessary. Scan images were reconstructed using the ordered-subsets expectation maximization algorithm (2 iterations, 14 subsets). Images were reconstructed into a 128 × 128 matrix with a pixel size of 2 × 2-mm. For lesion evaluation on PET imaging, we calculated a ratio between the maximum of standard uptake value (SUV) of PET tracer in lesions and the mean of SUV of PET tracer in the normal cortex in the opposite side of the brain (lesion/normal tissue (L/N) ratio) using Dr.View (INFOCOM CORPORATION, Tokyo, Japan).

MET and CHO L/N ratios before and after BEV therapy were measured in each case. The reduction rates of MET L/N ratio and of CHO L/N ratio were calculated by the formulas below.

Reduction rate of MET L/N ratio
= (MET L/N ratio before BEV therapy
− MET L/N ratio after BEV therapy)
/MET L/N ratio before BEV therapy

Reduction rate of CHO L/N ratio
= (CHO L/N ratio before BEV therapy
− CHO L/N ratio after BEV therapy)
/CHO L/N ratio before BEV therapy

Clinical evaluations

KPS, blood–chemical examinations, MRI, MRS, and PET were evaluated before and after BEV therapy. These clinical and radiological parameters after BEV therapy were obtained within 7 days after BEV therapy completion. For KPS, a score increase of 10 points or greater following BEV therapy was defined as improved.

Statistical analysis

Student's t test was used for statistical analysis to compare the KPS score, Gd-volume, FLAIR-volume, MET L/N ratio, and CHO L/N ratio before and after BEV therapy. Student's paired t test was used for the Cho/Cr ratio. Differences of $p < 0.05$ were considered statistically significant. All data were analyzed using SPSS 2 for Windows.

Diagnosis of RN

Radiological RN diagnosed by the criteria below was defined as RN. First, for Gd-MRI, newly enhanced lesions within areas previously irradiated for treatment were regarded as RN candidates. Additionally, for Gd-MRI, lesions showing a MET L/N ratio less than 2.51 were defined as RN and BEV therapy candidates. This criterion of MET-PET differential diagnosis was utilized in a previous MET-PET study by Takenaka et al. [13].

Results

MRI

Both Gd- and FLAIR-volumes of RN on MRI decreased in all patients after BEV therapy (Table 2). The mean size reduction rates were 80.0 and 65.0 % in Gd- and FLAIR-volumes, respectively (Table 2). RN radiological change on MRI of a representative case (Case 1) is shown in Fig. 1. The mean values of both Gd- and FLAIR-volumes before BEV therapy were 39.9 and 156.7 ml, respectively, and those after BEV therapy were 8.3 and 50.8 ml, respectively (Fig. 2). The mean values of both Gd- and FLAIR-volumes were significantly decreased after BEV therapy ($p = 0.01$ in Gd-volume and $p < 0.001$ in FLAIR-volume) (Fig. 2).

MRS

Mean Cho/Cr ratios of RN before and after BEV therapy in Case 2, 7, and 9 were 4.03 and 2.87, 3.76 and 1.93, and 3.90 and 3.44, respectively (Table 3). Mean Cho/Cr ratios after BEV therapy were significantly decreased in each of these three cases ($p < 0.07$, $p < 0.016$, and $p < 0.14$ in Case 2, 7, and 9, respectively) (Table 3; Fig. 3).

PET

RN MET and CHO L/N ratios decreased in 8 (89 %) and 9 patients (100 %), respectively (Table 2). Mean reduction rates of MET and CHO L/N ratios were 24.4 and 60.7 %, respectively (Table 2). Radiological change of RN on PET of a representative case (Case 1) is shown in Fig. 1. The mean values of MET and CHO L/N ratios of the 9 patients before BEV therapy were 2.19 and 9.24, respectively, and after BEV therapy were 1.71 and 3.19, respectively (Fig. 2). Mean values of MET and CHO L/N ratios significantly decreased after BEV therapy ($p = 0.01$ in MET and $p = 0.002$ in CHO) (Fig. 2).

Table 2 Clinical and radiological parameters of RN patients

Case	KPS before BEV therapy	KPS after BEV therapy	Gd-volume size reduction rate (%)	FLAIR-volume size reduction rate (%)	Initial MET L/N	MET L/N ratio reduction rate (%)	Initial CHO L/N	CHO L/N ratio reduction rate (%)
1	60	70	91.2	68.8	2.17	28.2	7.65	84.7
2	90	100	64.8	61.1	2.43	25.3	7.41	67.1
3	60	60	78.1	60.3	2.43	40.7	12.68	63.2
4	70	90	60.6	92.3	2.49	47.6	8.57	79.1
5	90	100	99.0	58.2	1.82	29.7	5.74	63.1
6	60	70	55.9	88.9	2.07	−9.2	20.27	70.8
7	90	100	43.2	65.0	1.91	26.2	7.64	65.7
8	60	60	73.5	25.6	1.89	6.9	4.28	3.5
9	50	70	81.1	64.6	2.50	23.9	8.94	49.2
Mean	70	80	80.0	65.0	2.19	24.4	9.24	60.7

RN radiation necrosis, *KPS* Karnofsky performance status, *BEV* bevacizumab, *Gd* gadolinium, *FLAIR* fluid attenuated inversion recovery, *MET* 11C-methionine, *CHO* 11C-choline, *L/N ratio* lesion/normal tissue ratio

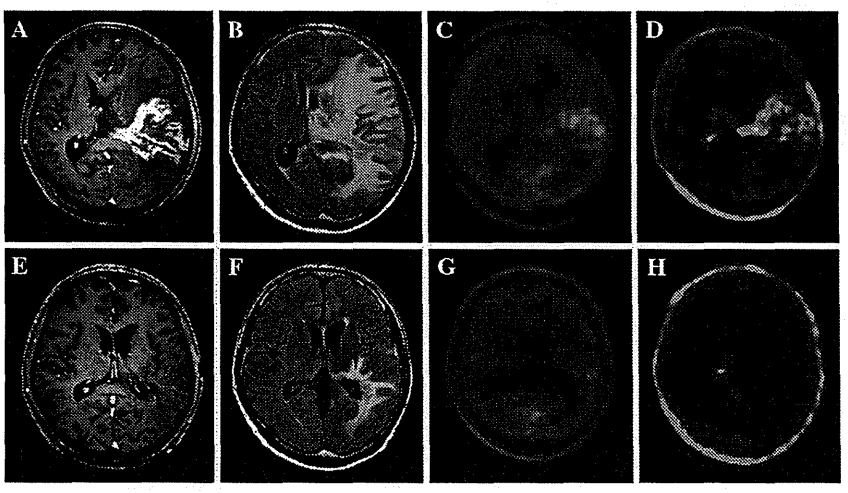

Fig. 1 MRI and PET radiological changes of the Case 1 lesion. An intensive Gd-enhanced lesion (**a**) and extensive abnormal high intensity area on FLAIR (**b**) is seen in the left cerebral hemisphere before BEV therapy. PET demonstrated that the L/N ratio of MET was 2.17 (**c**) and that of CHO was 7.65 (**d**). The Gd-enhanced lesion disappeared (**e**) and the abnormal high intensity area on FLAIR shrunk remarkably (**f**) after BEV therapy. The L/N ratios of MET and CHO substantially decreased to 2.03 (**g**) and 1.17 (**h**) after BEV therapy, respectively

Clinical effects and adverse events

KPS improved in 7 patients (77.8 %) after BEV therapy. Mean KPS scores before and after BEV therapy were 70 and 80, respectively ($p = 0.22$).

BEV-related adverse events of grade 1 or 2 occurred in three patients in which anemia, leukopenia, neutropenia, and lymphocytopenia were observed. High grade adverse effects (more than Grade 3) were not observed. In addition, no indications of previously reported severe adverse events related to BEV treatment, including cerebral hemorrhage or arterial thromboembolic events were observed.

Discussion

Discrimination of RN from tumor recurrence has been a demanding problem in clinical neuro-oncology and is practically important because these two pathologies require different treatments. Traditionally, the only method available to distinguish these two pathologies is histology. Recent advancement of metabolic neuroimaging modalities have made it possible to have a reliable RN diagnosis with both high specificity and sensitivity without tissue examination compared to conventional MRI. RN diagnosed by only neuroimaging (radiological RN) benefits patients since no

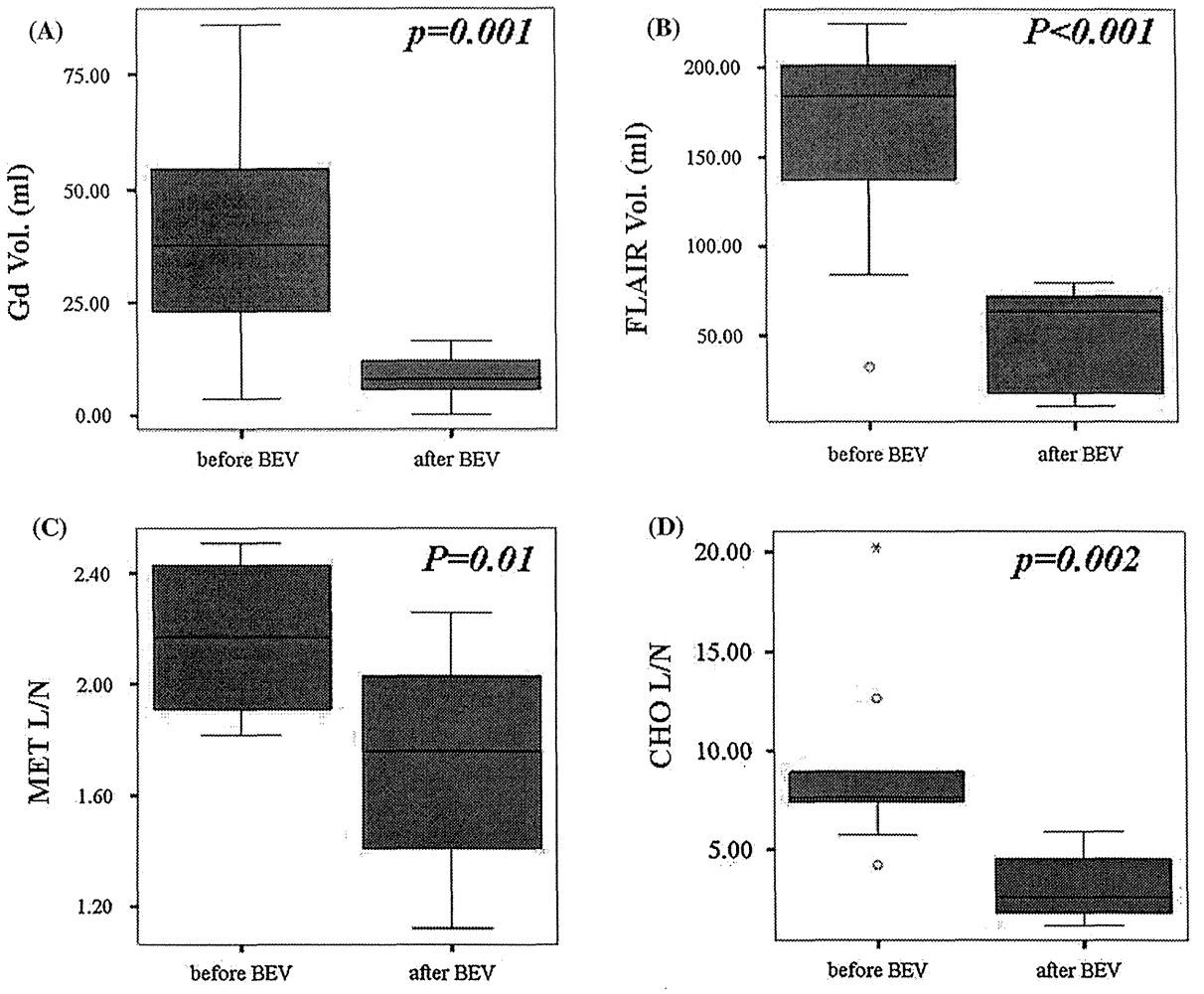

Fig. 2 Box-and-whisker plots outlining the distribution (mean and SD) of the Gd-volume (**a**) and the FLAIR-volume (**b**) of the lesion on MRI before and after BEV therapy, and those outlining the distribution (mean and SD) of the L/N ratios of MET (**c**) and CHO (**d**) of the lesion on PET before and after BEV therapy. The mean values of Gd- and FLAIR-volumes, and MET and CHO L/N ratios significantly decreased after BEV therapy

invasive intervention is then required for diagnosis and subsequent therapeutic decisions, though definitive diagnosis is not always possible with neuroimaging. In addition, there may be some scattered residual tumor cells within or around the RN lesions in cases of malignant gliomas, even if the lesions were reliably diagnosed with RN by histology. In this study, MET-PET was employed for radiological RN diagnosis based on Takenaka et al. [13].

Also in this study, BEV therapy led to a substantial decrease of RN volumes estimated by Gd-MRI and FLAIR and clinical improvements. These results were in agreement with the previous studies by Gonzalez et al. [7] and Levin et al. [8]. The principle therapeutic mechanism of BEV on RN has been thought to be relative normalization of the blood–brain barrier (BBB) attained by decreasing VEGF levels. From this study, another mechanism of BEV impact on RN growth suppression could be due to suppression of RN biological activities from BBB normalization. This proposed mechanism is based on MRS examination in this study and the resulting decrease in tissue metabolism.

Proton MRS is one modern modality for diagnosing and monitoring lesions by evaluating tissue metabolism. Generally, decreased Cho and *N*-acetylaspartate levels and increased lactate and lipid levels are the hallmark of RN [14]. On the other hand, in biologically active RN with progressing mass effect, relatively even Cho levels compared to malignant brain tumors can often be seen [15–17]. In all three cases in which MRS was performed in this study, Cho/Cr ratios were relatively increased before BEV therapy, and significantly decreased after BEV therapy.